4.0 EXPERIMENTAL RESULTS

This section begins with a description of the process control settings that were adjusted to match the target conditions specified for Test #1. Then representative results from every type of diagnostic are presented to illustrate the information that was monitored and collected on the ICET system for Test #1. This information is organized in categories relating more closely to operational activities than to diagnostic methods. For example, latent debris and chemical precipitates are presented in separate sections, even though SEM analysis was used for both types of sample. Data and photographs are provided here for the (1) coupon racks, (2) NUKON™ fiberglass samples, (3) concrete samples, (4) latent debris surrogate, (5) time-dependent solution chemistry, and (6) precipitated solids.

4.1 Test Operation and Sequence

4.1.1 Description

Preparation of ICET Test #1 (Run 1 in Table 2) began with the heating of 200 gal. of RO water to 60°C. Upon reaching the desired temperature, the premixed chemicals were added. Those chemicals consisted of boric acid, NaOH, LiOH, and HCl, which were added with the recirculation pump operating. After the chemicals were observed to be well mixed, an additional 50 gal. of RO water was added to reach the required test volume. The solution again was brought to the desired test temperature. Premeasured latent debris and concrete dust, metal coupons, and fiberglass samples then were put into the tank. After adding all required items into the tank, baseline grab samples and measurements of the test solution were taken.

Addition of the fiberglass and metal coupons took place on the evening of November 20, 2004. Because of the quantity of the metal mass added to the tank, the solution temperature dropped below the desired test range. The test apparatus was held in this state for approximately 12 hours until the next morning, when the temperature had again reached the desired value. Some settling of the added particulates was observed overnight, with the turbidity decreasing from 12 to 8 NTU over that time.

The experiment commenced at 10:00 A.M. on Sunday, November 21, 2004, and it ended on Tuesday, December 21, 2004, at 10:00 A.M. Time zero of the test commenced with initiation of the tank sprays, which lasted for 4 hours. During the first 30 minutes of the spray period, a chemical metering pump was used to inject, directly into the nozzle supply lines, additional NaOH into the solution. The total nozzle spray flow was 3.5 gpm, and the recirculation flow was set at 25 gpm. During the test, grab samples were taken on a daily basis for wet chemistry and ICP analyses. Water loss due to water sample removals and evaporation was made up with RO water. When the water inventory dropped to approximately 5% of the inventory (12.5 gal.), RO water was added to bring the inventory back to 250 gal. Over the course of the test, a total of 22 gal. of RO water was added, and the inventory at test termination was 239 gal. Post-test analyses of water samples, fiberglass, and metal coupons were performed. Sampling and analyses were conducted in accordance with approved project instructions.

4.1.2 Process Control

Process control consisted of monitoring online measurements of recirculation flow rate, test solution temperature, and pH. Flow rate and temperature were controlled to maintain the desired values.

Recirculation Flow Rate: The 30-day average recirculation flow rate was 95.2 L/min (25.1 gpm). The recorded recirculation flow rate had a standard deviation of 0.2 L/min, with a range of 94.3 to 98.2 L/min (24.9 to 25.9 gpm), excluding the spray cycle. Variations were slightly greater during the spray cycle

(range 88.8 to 99.1 L/min, or 23.5 to 26.1 gpm) because of the requirement to direct a portion of the flow manually to the spray nozzles.

Temperature: Temperature was recorded at three submerged locations in the ICET tank. The 30-day average recorded temperature at these locations was 60.1°C, 60.0°C, and 59.8°C (140.2°F, 140.0°F, and 139.6°F). The standard deviation in temperature recorded by all three thermocouples was within ±0.27°C (±0.48°F), with a maximum range of all thermocouples, of 58.5°C to 61.0°C (137.3°F to 141.8°F).

pH: The pH after initial chemical addition was complete was 9.1. During the 30 minutes of NaOH injection, the pH increased to 9.5. The pH value after NaOH injection was complete was within the range predicted by water chemistry calculations. The calculations predicted a pH between 9.4 and 10.0 at a standard temperature of 25°C. The low pH estimate was based on complete equilibration with atmospheric carbon dioxide (CO_2), and the high pH estimate was based on complete exclusion of atmospheric CO_2. Conditions during chemical addition favored the absorption of CO_2, resulting in a pH near the low end of the range. The conditions that favored CO_2 absorption were the result of actions designed to encourage boric acid dissolution. These conditions included (1) NaOH was added before boric acid, leaving the tank solution with a high initial pH; (2) the water level in the tank, as boric acid was being added, was below the level of the recirculation headers, thus creating a high degree of turbulence and also allowing intimate contact between air and water; and (3) the recirculation pump was operated at 390 L/min (103 gpm) as boric acid was being added, which increased turbulence and encouraged the entrainment of air.

4.1.3 Hydrogen Generation

As a safety precaution, the vapor space of the test apparatus was monitored daily for the presence of hydrogen gas. Measured concentrations never were observed to exceed the action level for flammability safety. Hydrogen concentrations were monitored for safety reasons only and cannot be interpreted quantitatively because (1) the tank lid was continuously but passively vented through two 3/4-in.-diam ball valves, (2) samples were taken through a plastic tube inserted through one of the valves so that the gas sample was extracted near the top of the tank, (3) no provisions were made for mixing gas in the well-insulated head space, and (4) the handheld hydrogen detector that was used provided sufficient sensitivity to avoid a safety concern but not sufficient accuracy to be used for quantitative assessment. Despite these limitations, it is instructive to note that nearly constant hydrogen levels were observed for the first 17 or 18 days of the test, and then the observed levels began to decline. For the last 5 days of the test, the hydrogen level was undetectable under the procedure described above.

4.2 Coupon Racks

The total of 373 metal coupons and 1 concrete coupon was contained in the tank during Test #1. Coupon types consisted of aluminum, copper, galvanized steel, carbon steel, and steel coated with inorganic zinc (IOZ) primer. Those coupons were loaded in seven coupon racks, with the numbering configuration shown in Figure 16. Racks #2 through #7 were exposed to the nozzle spray for the first 4 hours of the test. The nozzles were designed and oriented to provide a uniform, even spray over the racks. Following the spray phase of the test, those racks were left in the humid tank environment, and water drops were observed falling from the coupons and racks.

Coupon rack #1 was positioned so that it was submerged for the entire 30-day test. It remained located between the two recirculation flow headers in the tank to expose the coupons to a fairly uniform flow rate across their surfaces.

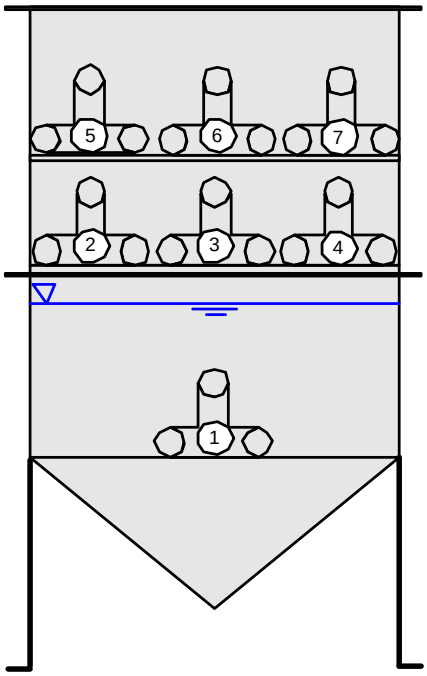

Figure 16. Coupon rack configuration in the ICET tank.

4.2.1 Physical Observations

All of the coupons were weighed before and after the test, photographed, inventoried, and stored. The surface appearance of the submerged coupons was changed considerably more than the non-submerged coupons.

Figure 17, looking down into the tank, shows portions of coupon racks #2 through #4 before test initiation. A SS mesh holder containing a fiberglass sample is shown on the end of rack #3. The angle iron shown above the racks is where racks #5 through #7 will rest. Figure 18 shows one of the coupon racks being hoisted into the tank before test initiation. Figure 19 shows the typical appearance of the unsubmerged racks after their removal from the tank.

Figure 17. Coupon racks inside ICET tank before start of test.

Figure 18. Coupon rack being loaded into the ICET tank.

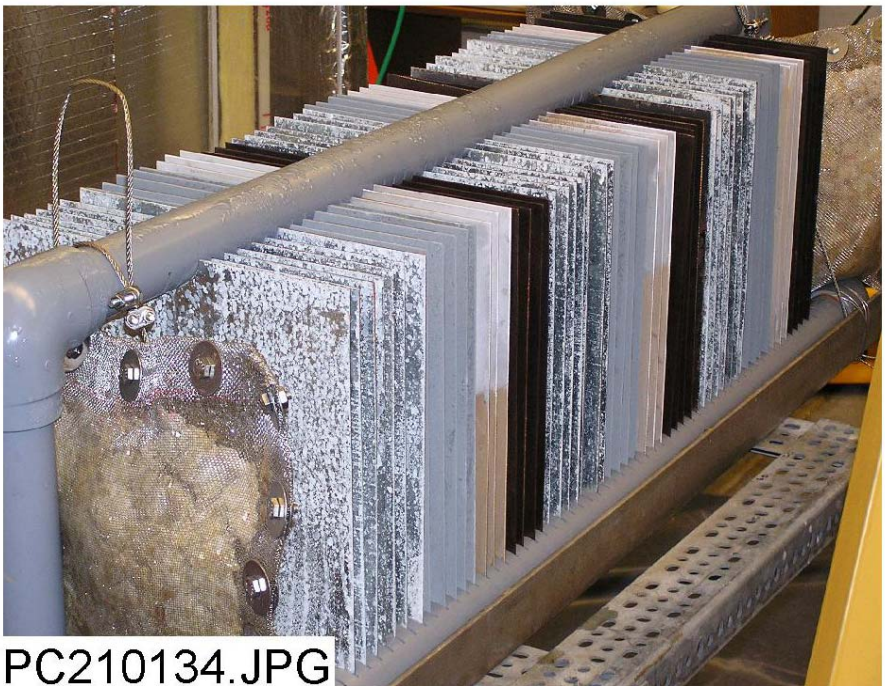

Figure 19. Coupon rack following removal from the ICET tank.

4.2.2 Weight Measurements

Measurements of coupon weights were taken on a calibrated scale. Weight differentials less than 0.1 g are within the measurement uncertainty, and measurements less than 1 g should be used as qualitative indicators of change.

4.2.2.1 Submerged Coupons

In one coupon rack, forty coupons were submerged in the chemical solution. Of these coupons, 25 were copper (average weight of 1317.7 g), and 24 of these experienced changes in weight that ranged between 0.0 g and 0.1 g. One copper coupon gained 2.0 g. That value appears to be an outlier, possibly caused by a faulty measurement. Weight changes for the seven galvanized steel coupons (average weight of 1054.83 g) ranged from 0.04 g to 0.06 g. The three IOZ-coated steel coupons (average weight of 1625.2 g) were less than 0.1 g. The three aluminum coupons (average weight of 392.0 g) experienced an average weight loss of 98.61 g. The single uncoated carbon steel coupon lost 23.3 g from an original weight of 1025.2 g. The concrete coupon gained 233 g from an original weight of 8586 g, possibly from retaining excess water that was not liberated after several days of air drying at room temperature.

4.2.2.2 Unsubmerged Coupons

Weight differentials (value of final weight minus initial weight) for the unsubmerged coupons were much smaller than those of the submerged coupons, and they varied between small positive and negative values. A total of 334 coupons were unsubmerged and were contained in 6 coupon racks. The distribution of coupon materials was 127 galvanized steel, 75 copper, 74 coated steel, 56 aluminum, and 2 uncoated carbon steel. The mean weight differential of the two carbon-steel coupons was 0.2 g. The maximum weight gains experienced by the remaining unsubmerged coupon materials are summarized in Table 4.

Table 4. Range of Weight Gains for Each Unsubmerged Coupon Material Type

Material	No. of Coupons	Maximum Gain (g)
Coated Steel	74	2.3
Aluminum	56	1.9
Galvanized Steel	127	0.7
Copper	75	0.4

It should be noted that the greatest single weight differential of 2.3 g on a coated steel coupon is ~0.14% of the original weight.

4.3 NUKON™ Fiberglass Samples

One of the common types of insulation used in nuclear power plants is NUKON™ fiberglass insulation, which is composed of a glass compound with various oxides and a binder. The glass composition of Owens Corning's NUKON™ insulation is given in Table 5 (data provided by the manufacturer). The NUKON™ fiberglass provided for the ICET tests was heat treated and shredded. Note that the information in the following two paragraphs was provided by the NUKON™ manufacturer.

Table 5. NUKON™ Glass Composition

Oxide	Maximum, %	Minimum, %
SiO_2	64.4	60.6
Al_2O_3	4.4	2.8
CaO	8.7	7.7
MgO	3.7	3.2
Na_2O	16.7	14.9
B_2O_3	5.8	4.2

According to the manufacturer, the binder on the NUKON™ Base Wool is a phenolic resin binder that starts decomposing at about 400°F and is probably totally decomposed at 600°F. After heating this insulation material on a 600°F hot plate for several hours, typically one-third of the binder decomposes into thermal decomposition gases, which represents the weight loss. Because the unheated NUKON™ Base Wool has 3% binder content by weight, the insulation material loses approximately 1% of its weight through heating on a hot plate.

Also according to the manufacturer, the binder left on the insulation has some discoloration, particularly in the transition zone between that on the yellow, cold insulation side and that on the white, hot insulation side (white indicating total binder loss and yellow indicating zero binder loss). In this transition zone, the binder is partially decomposed and the discoloration includes the color brown. The exact chemical identity of this brown, partially decomposed binder is not known, nor is its solubility in a water-based solution, such as boric acid. However, it is likely that this partially decomposed binder would discolor the boric acid solution into which it has been placed. It is not likely that the discoloration of the boric acid solution is caused by the glass fibers themselves because of the fact that this leaching process would have resulted in an apparent build-up of the discoloration that was not observed. Likewise, it is not likely that

the binder on the cold insulation side would dissolve in the boric acid solution and contribute to its discoloration.

For Test #1, 4.58 ft^3 of NUKON™ fiberglass enclosed in a fine SS mesh was placed in the tank. Of this amount, 75% was submerged below the water level and 25% was placed above the water level and exposed to sprays. The fiberglass had been heated before the test, as described above, to remove in part the organic binder in a manner consistent with the service life of similar products found in containment.

4.3.1 SEM/EDS

Fiberglass debris is encased in SS mesh bags to minimize migration throughout the tank. Small SS mesh envelopes approximately 4 in. square containing approximately 5 g of fiber are pulled out of the tank periodically for SEM examination. These sample envelopes are placed in a range of water flow conditions, but none have direct water flow through the fiber, and all are thoroughly immersed in the test solution until they are recovered from the tank. After exposure for some period of time, deposits are formed throughout the fiber matrix that appear to be of chemical origin. SEM images show that various structures formed on the fibers are similar for the Day-15 and Day-30 test samples. However, coverage and thickness of deposits are more advanced in the Day-30 samples. Fiberglass material extracted from the surfaces of larger clumps shows the greatest buildup, whereas fibers on the interior of larger clumps appear to be almost unaffected.

Several different deposition structures are observed on the fibers, progressing in coverage from individual particles deposited on each fiber to sheets of film and very thin crusts that stretch between multiple fibers. When viewing the following photographs, note that all samples are thoroughly desiccated before examination. Figure 20 shows an SEM image for a pretest sample of fiberglass. The fibers are clean, with no particles deposited on them. Figure 21 shows a Day-15 test sample, where particles are beginning to deposit on the fibers. Figure 22 shows an SEM image for a Day-30 test sample. Sheets of thin film are forming over and between the fibers. Figure 23 shows an SEM image for a Day-15 test sample that illustrates similar deposits between fibers. The deposits observed in these samples appear to be capable of changing the head-loss characteristics of a fiber bed, but it has not been conclusively demonstrated that similar deposits would form under directed water flow similar to that present at the face of a sump screen.

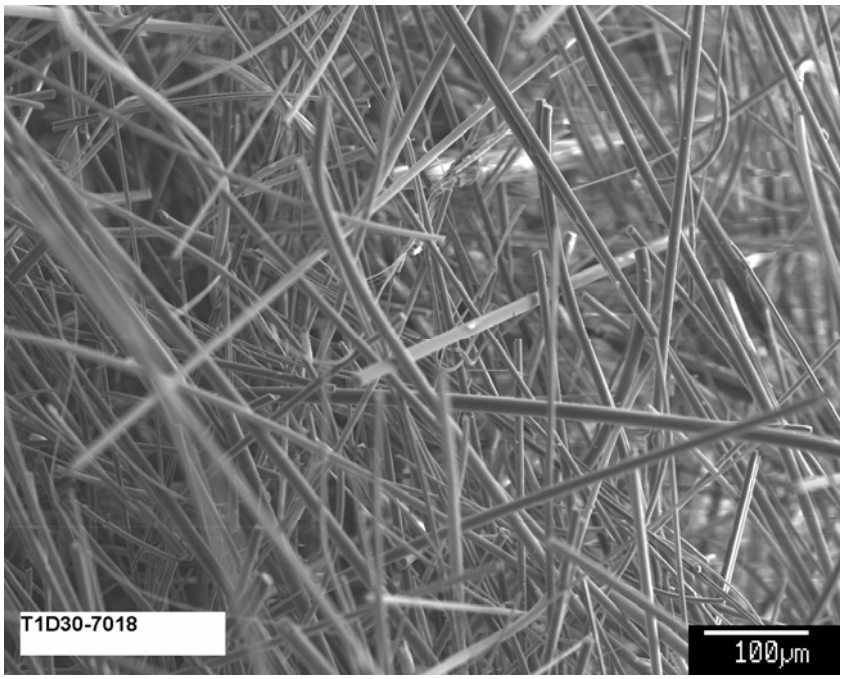

Figure 20. SEM image for a pretest sample of clean fiberglass.

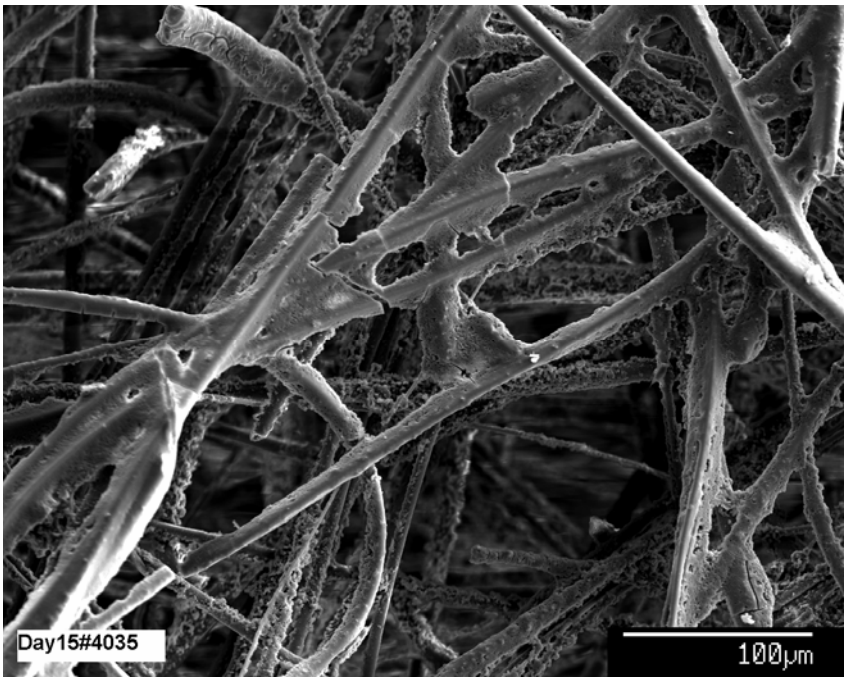

Figure 21. SEM image for a Day-15 test sample illustrating crusty deposits or growth on fiberglass.

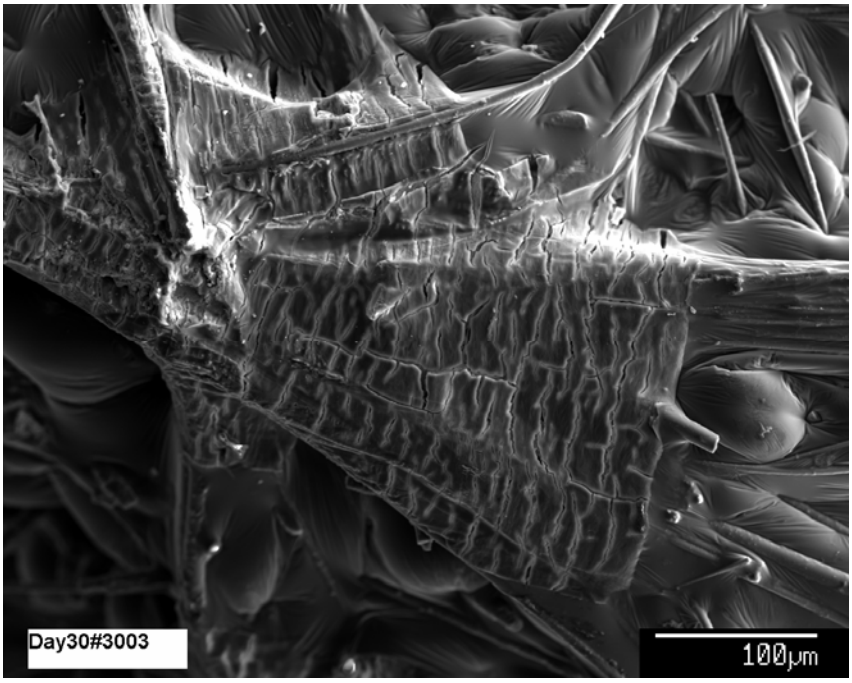

Figure 22. SEM image for a Day-30 test sample illustrating membrane films deposited between fibers.

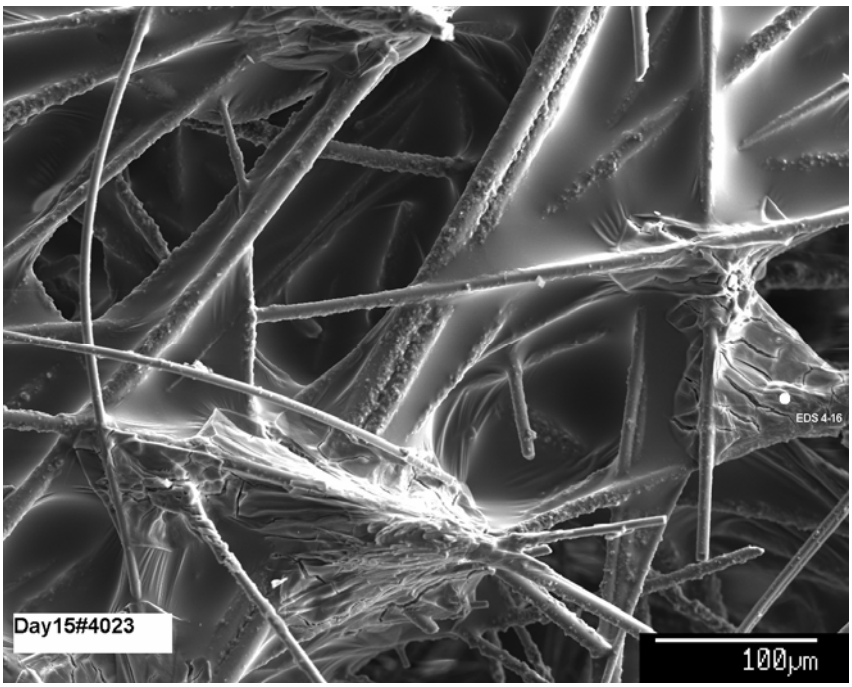

Figure 23. SEM image for a Day-15 test sample (sample #4023) magnified 230 times, illustrating deposits between fibers.

Figure 24 shows a typical EDS spectrum for a Day-15 test sample. This particular sample is dominated by oxygen and sodium. These test samples typically contain various elements, such as carbon, oxygen,

sodium, magnesium, bromine, silicon, calcium, manganese, iron, and zinc. It should be noted that gold (Au) and palladium (Pd) are present in almost all EDS spectra because of the sputtering technique used to prepare the SEM samples. The highly conductive sample surface provided by metallic sputtering prevents charge buildup under the electron beam that would destroy image quality. Peak counting intensities are proportional to elemental concentration but must be compensated by the energy-dependent detector response function and normalized to an assumed set of elemental constituents before proportional compositions can be inferred. Further explanation of EDS spectra and many additional examples are provided in the appendices, including many with accompanying composition analyses.

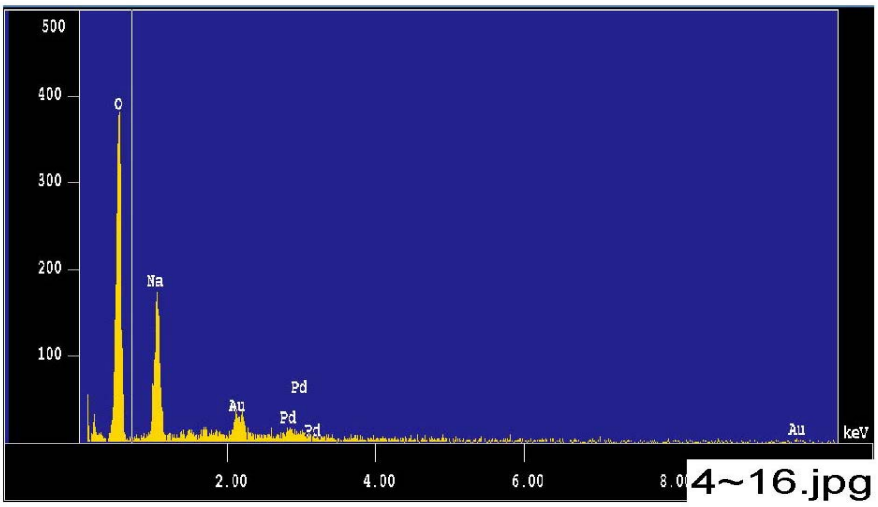

Figure 24. Day-15, sample #4 counting spectrum (EDS 4-16) taken for the cracked deposits at the right-hand side of Figure 23.

4.4 Concrete Samples

A scaled amount of concrete and its aggregate were ground up into dust. The amount used for the 250-gal. test volume was 21.2 g. In addition to the concrete, 63.7 g of a latent debris surrogate was prepared. The surrogate consisted of three size distributions and two different materials. Sand was used for the two larger sizes, which were 0.075–0.59 mm and 0.59–2 mm, respectively. These two sizes accounted for 35% and 28% of the total added. Clay was used for the smallest size, which was <0.075 mm. The concrete dust and latent debris were added to the test solution just before the start of the test.

4.5 Solution Chemistry

Daily water samples were extracted from the ICET tank in accordance with written instructions. Portions of these samples were archived in airtight plastic bottles for longer duration observation and analyses. Each sample was identified by a four-field tag containing the ICET acronym and test number, the date of extraction, the time of extraction, and the filtration status (U for unfiltered, F for filtered). For example, an unfiltered sample collected on November 20 at 5:03 P.M. would be labeled as ICET-1120-1703-U.[1] Figure 25 illustrates the water sample collection process.

[1] Slight variations on this nomenclature have been used to label filter papers and other solid samples. For example, tags such as T1D30 have sometimes been used to designate Test #1, Day 30.

Figure 25. Daily water grab sample extraction.

4.5.1 Water Color

After chemical addition but before placement of coupons, fiberglass, and debris, the water was clear. After placement of the coupons, fiberglass, and debris, the water had a distinct yellow color. Even after particulate debris settled in the tank and the turbidity and TSS dropped to low levels, the yellow color remained. Examination of the stored sample bottles reveals that the color qualitatively remained nearly constant over the duration of the test, although the final day or two may have been slightly less yellow than the previous days. The precipitation and settling of solids in the stored bottles did not appear to have had a significant impact on the color. Although several sources for this color are possible, the most likely source is the fiberglass insulation, based on an evaluation of the materials in the tank. The NUKON™ fiberglass placed in the tank was yellow, and the vendor of the fiberglass indicated that the yellow color was due to the presence of a phenolic resin binder. No other materials placed in the tank had a yellow color. Corrosion products from metal coupons can be colored, but of the materials placed in the tank, only iron oxides will produce color similar to the color observed in the tank, and the iron concentration was below the detection limit in the solution.

Figure 26 and Figure 27 illustrate the bench-top measurement area used for tests on water samples.

Figure 26. Wet chemistry analyses.

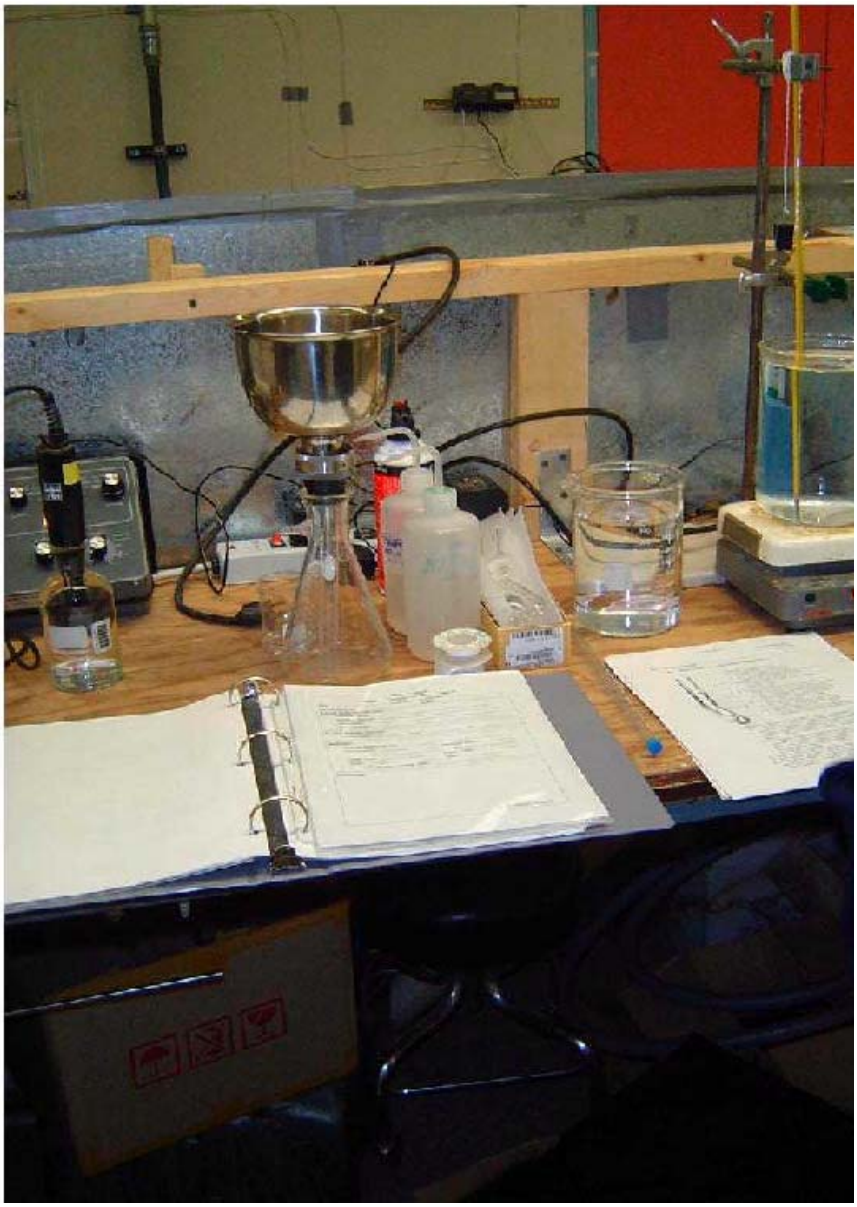

Figure 27. Bench-top water sample characterization.

4.5.2 Turbidity

Figure 28 displays the turbidity trend observed during Test #1. There are 3 different values shown on the plot for time zero. The first point was taken after adding chemicals, concrete dust, and latent debris but before adding coupons or fiberglass. The turbidity was then measured to be 0.61 NTU. After adding the sample coupons and fiberglass samples, the solution was murky and it was impossible to see more than a couple of inches into the tank. The measured turbidity at that point was 12 NTU. The next morning, the turbidity had decreased to 8 NTU. Following the start of the test, turbidity was measured to be 14.4, 13.3, 11.4, and 8.3. Those values were at 0.5, 2, 4, and 8 hours, respectively, after the test start. At 24 hours, the turbidity had dropped to 1.3 NTU, and it continued to drop over the next two days, reaching a value of about 0.3 NTU by Day 3. The turbidity remained relatively steady throughout the remainder of the test.

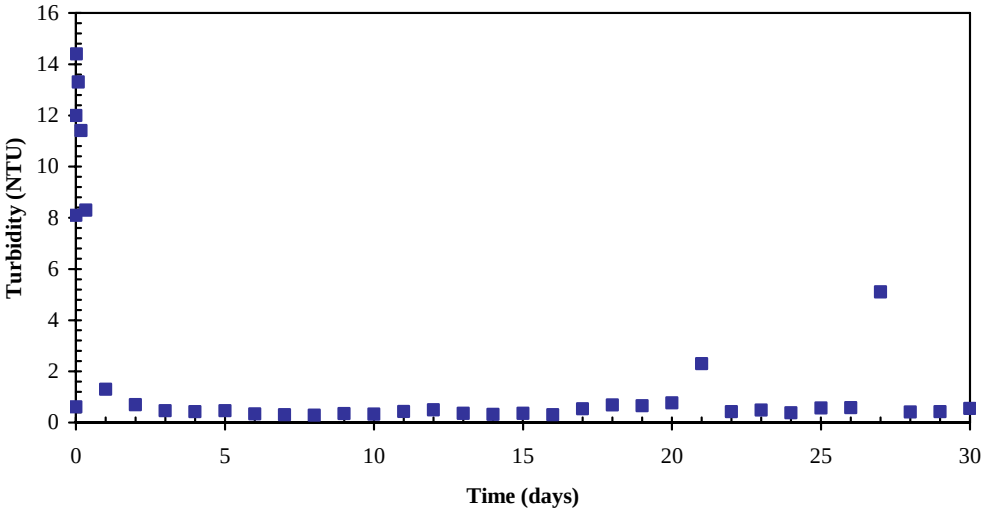

Figure 28. Turbidity trend at the test temperature observed during ICET Test #1.

Turbidity values were measured while the solution was still near the process temperature of 140°F. It was observed that the precipitation that occurred in the sample solution was very time- and temperature-sensitive. Therefore, lapses of just a couple of minutes would cause a higher turbidity reading, which appears to be the case for the values at 21 and 27 days shown in Figure 28. A longer period of time may have elapsed between the sample taking and the measurement.

The turbidity values shown in Figure 28 were measured while the solution was still near the process temperature of 140°F. The test plan also included a requirement to measure turbidity at ambient temperature [23 (±2.0) °C], which is presented in Figure 29. During the first day, turbidity at ambient temperature was identical to turbidity at process temperature. However, on Day 2, it was noted that turbidity at ambient temperature was higher than at process temperature. It was also noted on Days 2 and 3 that the turbidity at room temperature was time dependent and increased as the holding time increased. Therefore, a procedure was implemented on Day 4 that required the ambient-temperature turbidity to be recorded after a cooling time of 10 minutes. The 10-minute ambient-temperature turbidity asymptotically increased over the duration of the test, reaching a value of 133 NTU by Day 30. The cause of the rapid rise in turbidity while cooling was attributed to a white, finely divided precipitate that gradually settled to the bottom of the sample storage bottles.

The presence of precipitate in the 10-minute daily samples indicates that the tank solution reached room-temperature saturation of at least one species very rapidly. Post-test examination of the stored water from the daily samples indicates that the quantity of precipitate continued to increase as testing time progressed. The amount of precipitation appears to be temperature and time dependent. Water held at 60°C was never observed to form precipitates, but when the water is cooled to 23°C, precipitates form gradually over time.

Turbidity appears to be a sensitive indicator of the rate of the precipitation reaction. As the water cooled from 60°C to 23°C, the turbidity was observed to increase from 0.3 NTU to more than 133 NTU in a 10-minute period. In addition, the viscosity results at 23°C are more variable (see Section 4.5.5). As with turbidity after Day 2, viscosity was time and temperature dependent. It was not possible to hold each viscosity sample for the exact same amount of time before taking the measurement at 23°C.

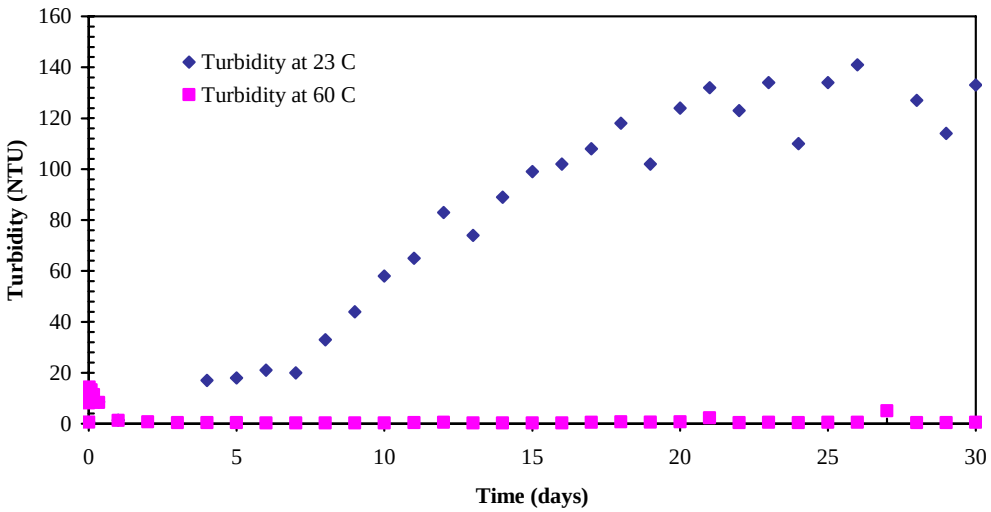

Figure 29. Turbidity measured at 23ºC and 60ºC during ICET Test #1.

4.5.3 Total Suspended Solids

Total suspended solids (TSSs) are measured by filtering a volume of approximately 500 mL through an in-line, 0.7-µm, glass microfiber filter directly at the sample tap and drying and weighing the filter paper to determine what was collected. The selected equipment and procedure ensure that TSS measurements are not affected by temperature-dependent or time-dependent precipitation reactions that may occur once the process solution is removed from the tank. The TSS concentration was 27 mg/L after the coupons, fiberglass, concrete dust, and latent debris were introduced to the tank. The next morning, the concentration was 29 mg/L. Values were 43, 32, 27, and 23 mg/L at 0.5, 2, 4, and 8 hours, respectively, after the test start. The TSS started dropping after the NaOH spray cycle was complete, reaching 27 mg/L at the end of the 4-hour spray cycle. TSS continued to drop during the test, which is consistent with the turbidity measurements. During Days 2 through 12, the TSS stayed low and within the range of 10 to 25 mg/L. From Day 13 to the end of the test, the TSS concentration rose but stayed consistently between 19 and 29 mg/L. The standard deviation in the measurement was experimentally obtained to be approximately 3 mg/L. An evaluation of variability outside of that number was not performed. The TSS concentrations are shown in Figure 30

On the last day of the test, 1 L of the end-of-test solution was taken for TSS analysis. The solution was shaken and then divided into seven samples that were held at different temperatures, ranging from room temperature (22.8°C) to 55°C. The solution was left at the desired temperatures for 72 hours before being filtered for TSS analysis. Various laboratory ovens and one water bath were used to control the temperature of the various containers so that analysis could be performed in a timely fashion. The desired temperatures ranged from room temperature to 60ºC, decreasing in 5ºC increments.

Figure 31 presents the results from this test. The TSS concentration increased relatively linearly, from approximately 100 to nearly 1800 mg/L as the constant sample temperature decreased from 55°C to 22.8°C.

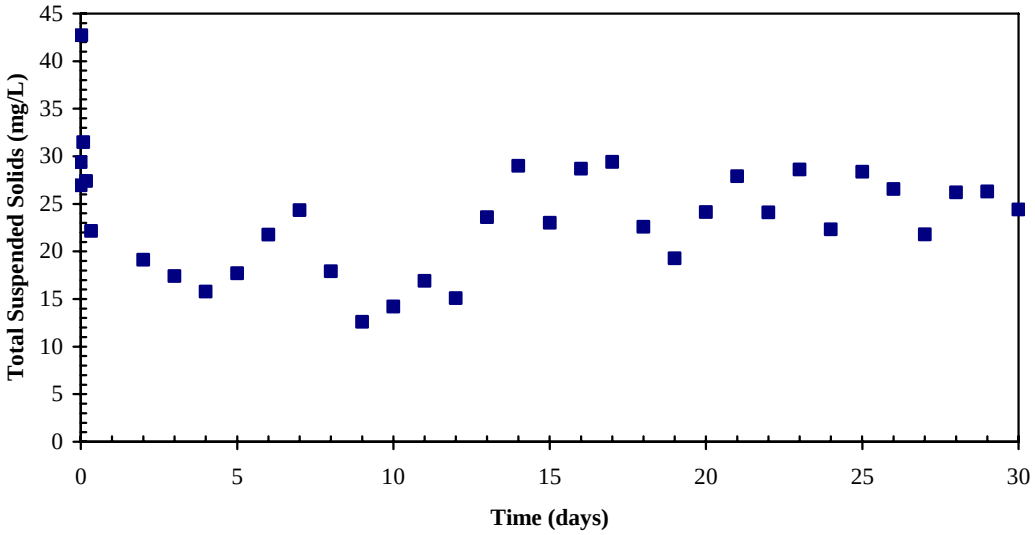

Figure 30. Total suspended solids during ICET Test #1.

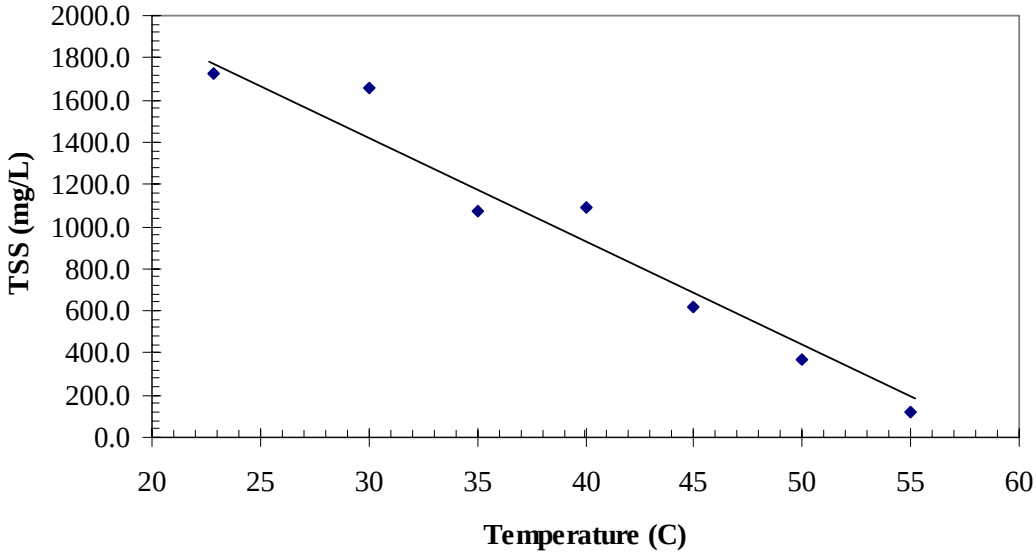

Figure 31. TSS results for the end-of-test precipitation experiment.

A similar study was conducted to determine if the precipitate that formed in the end-of-test solution upon cooling would redissolve into solution upon reheating to the test temperature. Several assumptions apply to this study:

1. The end-of-test solution is homogenous.
2. No change has occurred within the solution while being stored for 30 days at room temperature.
3. Temperature variation between heating baths and ovens used is negligible.

One-L bottles of end-of-test solution were subjected to constant desired temperatures for 72 hours. After 72 hours, the solutions were vigorously shaken to provide a homogenous sample that was then filtered for TSS analysis.

For reheating of the end-of-test solution, only one water bath was used to control the temperature because of the unavailability of the laboratory ovens. The only exceptions to this practice were the 60ºC and room temperature samples. The same 1-L sample bottle was placed in the water bath at the desired temperature for 72 hours. After 72 hours, a 100-ml sample was taken from the well-shaken 1-L sample bottle. The 1-L sample bottle, minus the volume taken for sampling purposes, was returned to the water bath. The water bath was adjusted to the required temperature for the next step in the experiment. The desired temperatures ranged from room temperature to 60ºC, increasing in 10ºC increments. See Figure 32 for the resulting TSS as a function of temperature.

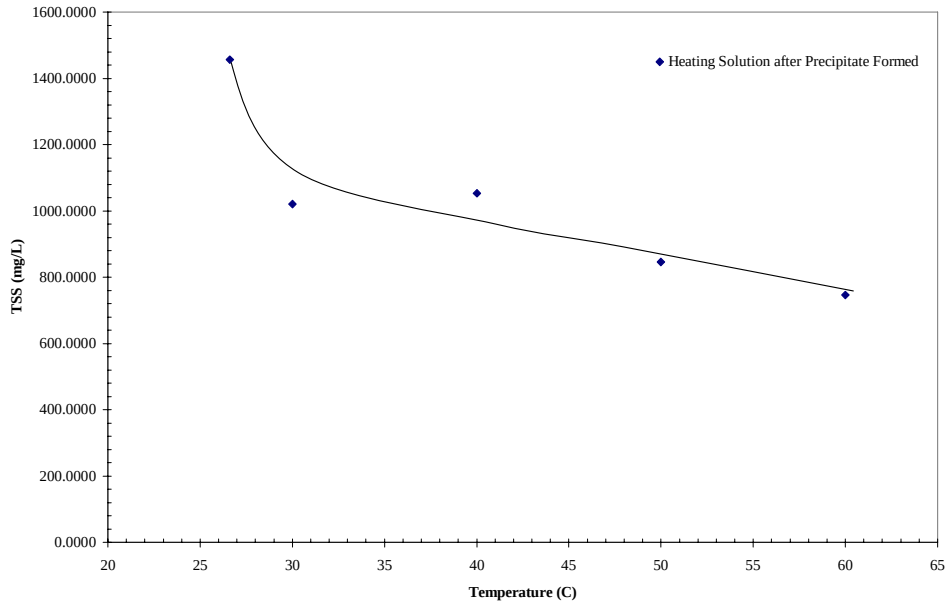

Figure 32. Temperature-precipitate relationship upon heating the end-of-test solution after precipitate has formed.

While the end-of-test solution was cooling, precipitates formed in a linear fashion with varying temperature, as seen in Figure 31. After the precipitate formed, heating of the solution caused some of the precipitate to redissolve into solution, as seen in Figure 32. Figure 33 displays the distinct difference in precipitation concentration due to heating and cooling of the solution. Also, from Figure 33, it can be seen that not all of the precipitate returned to solution when the test temperature is reached. The standard deviations of the results are unknown because of time constraints, so further testing must be done to correctly quantify precipitate concentrations under these time and temperature profiles.

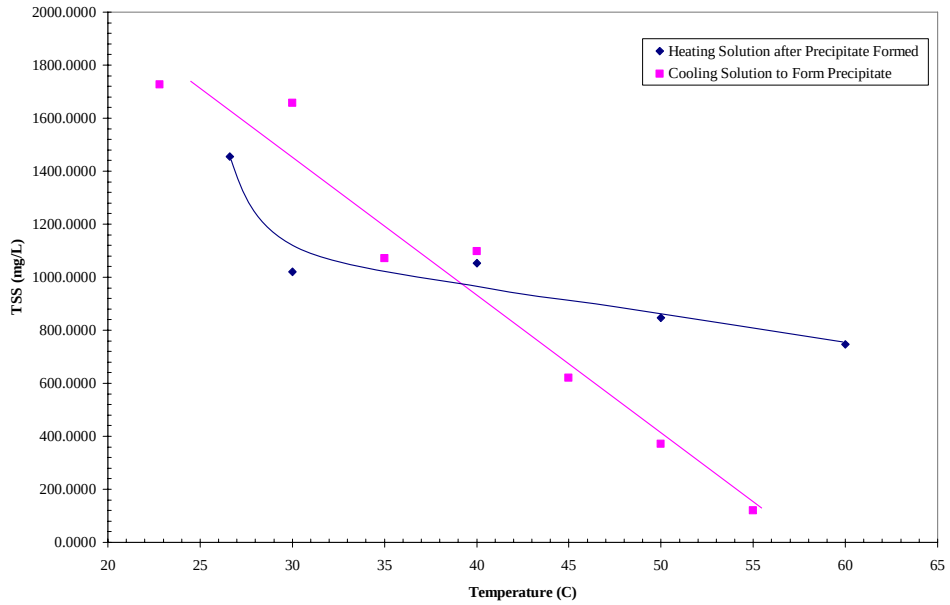

Figure 33. Temperature-precipitate relationship upon cooling and heating of end-of-test solution.

4.5.4 pH

As shown in Figure 34, the pH slowly decreased over the duration of the test. By the end of the test, the grab sample pH and the DAS pH differed from each other by approximately 0.10 pH units. The grab sample pH decreased from pH = 9.5 to pH = 9.35, whereas the DAS pH decreased from pH = 9.5 to pH = 9.28. This slight decrease in pH may have been caused by adsorption of additional atmospheric CO_2 or by corrosion reactions that resulted in the production of acid.

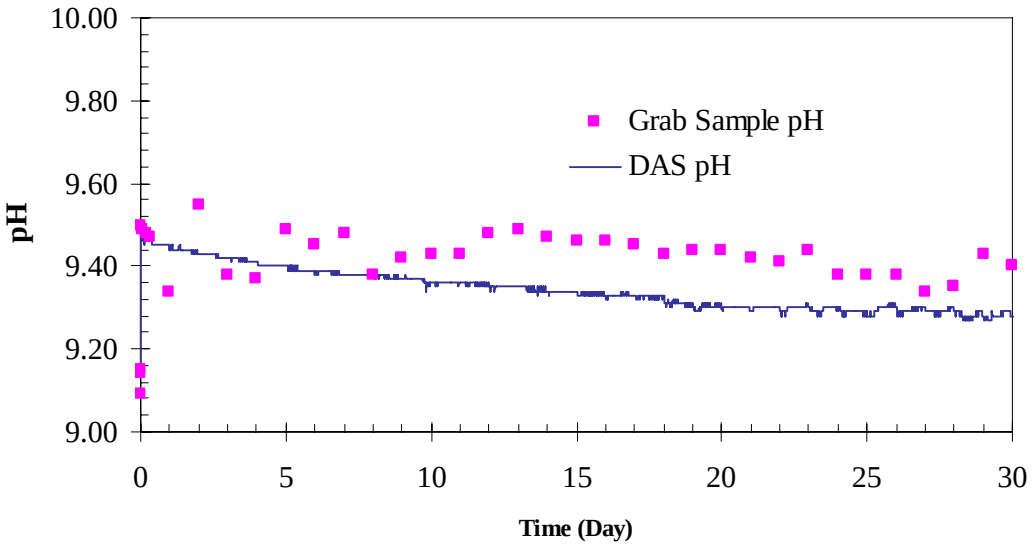

Figure 34. pH trend observed during ICET Test #1.

4.5.5 Constant-Shear Kinematic Viscosity

The viscosity of filtered and unfiltered solutions at 60.0°C is shown in Figure 35. Filtered and unfiltered viscosity at 60.0°C remained virtually unchanged. The filtered viscosity had a standard deviation of 0.014 mm^2/s (average = 0.514 mm^2/s, range = 0.469 to 0.552 mm^2/s) over the first 24 days of the test. Thus, on Day 25 of the test, filtered viscosity measurements were discontinued. The unfiltered viscosity had a standard deviation of 0.01 mm^2/s (average = 0.514 mm^2/s, range = 0.482 to 0.560 mm^2/s) through the duration of the test.

A slight increase in the viscosity measurements was observed from Day 11 through Day 14, and it was noticed that the viscometer contained visible residue after the standard cleaning procedure was completed. On Day 15, the viscometer was cleaned in an acid bath before use and the viscosity returned to the previous expected value. Thereafter, the viscometer was cleaned with acid after each measurement for the duration of the test.

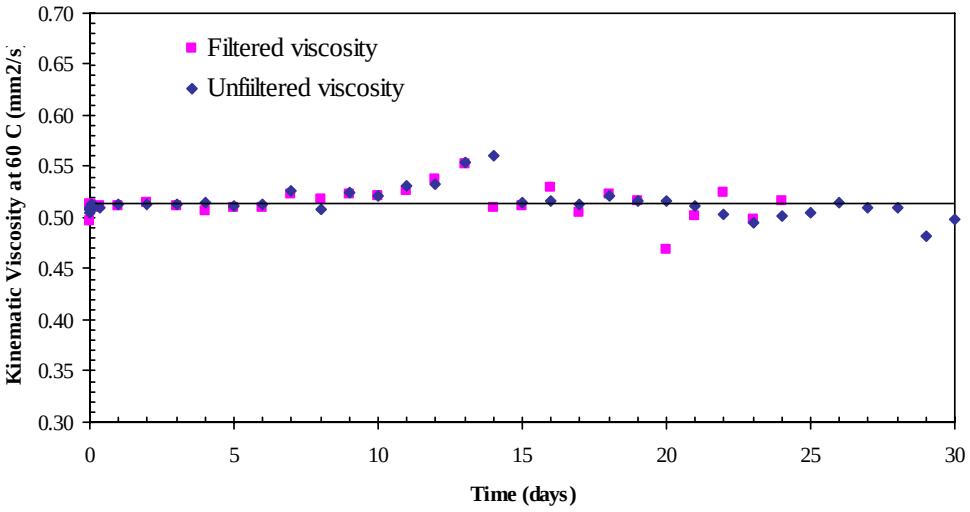

Figure 35. Kinematic viscosity of solution in ICET Test #1 at 60.0°C.

The viscosity of filtered and unfiltered solutions at 23.0°C is shown in Figure 36. Viscosity at 23.0°C has been more variable than viscosity at 60.0°C. This variability can probably be attributed to the time-dependent precipitation of solids at ambient temperature that was observed in the turbidity measurements. Over the duration of the test, the viscosity at 23.0°C gradually increased. The onset of precipitation of solids as a function of cooling also advanced over the test duration, which could account for the increase in viscosity observed under the established test procedure. The filtered viscosity had a standard deviation of 0.235 mm^2/s (average = 1.208 mm^2/s, range = 0.962 to 1.713 mm^2/s) over the first 24 days of the test. Again, on Day 25 of the test, filtered viscosity measurements were discontinued. The unfiltered viscosity had a standard deviation of 0.249 mm^2/s (average = 1.240 mm^2/s, range = 0.959 to 1.745 mm^2/s) through the duration of the test.

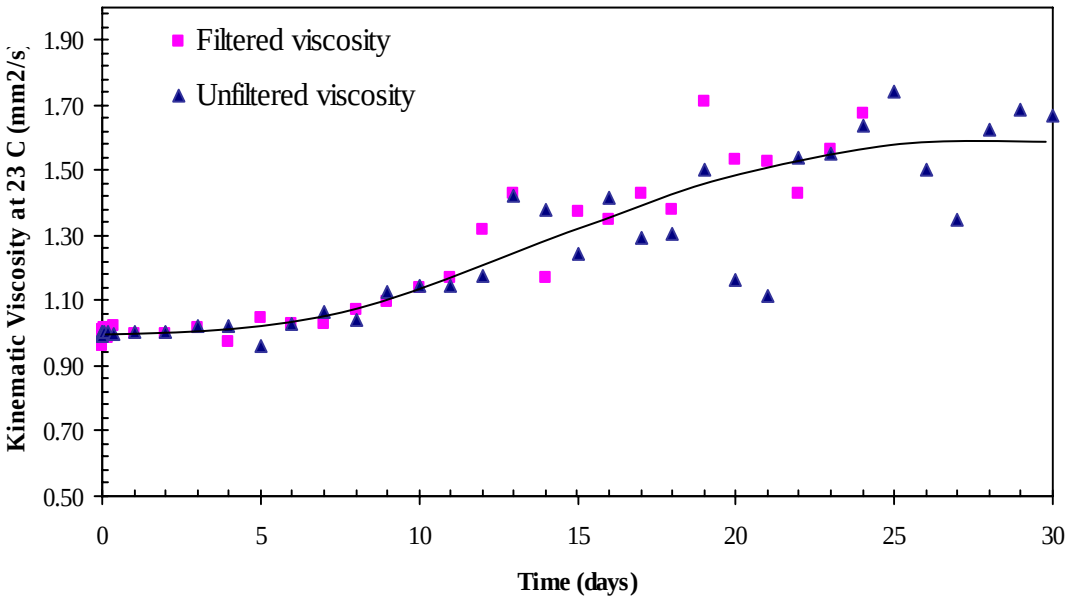

Figure 36. Kinematic viscosity of solution in ICET Test #1 at 23.0°C.

4.5.6 Shear-Dependent Viscosity

Newtonian fluids such as pure water are characterized by the constant proportionality between shear stress and deformation rate. This constant of proportionality is defined as the dynamic viscosity, μ. Most SolGels and gelatinous hydrated reaction products exhibit non-Newtonian behavior such that the deformation rate depends on shear stress in a nonlinear manner. For example, a non-Newtonian fluid may flow readily under low strain rates but respond more rigidly to resist high strain rates and vice versa. Thus, the measurement of shear-dependent viscosity can provide a sensitive indication of the presence of gelation or gel precursors. Shear-dependent viscosity of the tank solution (both filtered and unfiltered) was measured at several time points during Test #1. Results are presented and compared in this section for all time points in a comparison plot; however, basic trends are illustrated using the Day-30 sample results.

A Bohlin CS10 Controlled Stress Rheometer (also called a viscosimeter) was used to measure the shear-dependent viscosity. The instrument was calibrated, and a trained operator followed the manufacturer's instructions to obtain the actual measurements.

All measurements were conducted with a shear-stress range of 0.0095 to 0.12 Pa. Samples were measured at 60ºC first and then cooled to 25ºC. The samples were transported to the Bohlin CS10 Rheometer via a cooler containing a hot-water bottle to maintain a warm temperature. Any samples that were not immediately analyzed were placed into an oven set at 60ºC until they could be measured according to procedure. When samples were placed in the rheometer, their temperatures were controlled to the desired value. Through this procedure, the test sample was maintained continuously at the desired temperature.

Samples analyzed for shear stress viscosity are referenced using the following nomenclature. Results labeled "10am" were obtained on November 21, 2004, at 10:00 A.M. Results labeled "1800" were

obtained on November 21, 2004, at 6:00 P.M. “10am” corresponds to the start of Test #1, and “1800” corresponds to t = 8 hours into the test. Results labeled “1206-F” and “1206-U” are used for the water samples collected from the tank on December 6, 2004, that were filtered and unfiltered, respectively. Similarly, results labeled “1214” and “1220” are used for water samples collected from the tank on December 14, 2004, and December 20, 2004, respectively.

General Observations:

1. When the 25ºC measurements were taken, it was necessary to allow the samples to reach an equilibrium condition at the new temperature. If the measurement was taken too quickly, then a curve similar to the high temperature result was obtained.
2. The 1214 series samples exhibit Bingham-plastic flow.
3. The 1800 and 10 A.M. samples were measured at higher shear stresses than the 1206 series, while the viscometer was being set to capture the characteristics of the sample and the instrument settings adjusted to their appropriate ranges. Consequently, the 10 A.M. sample was discarded because it was nearly the same as the 1800 series.

The following plots illustrate basic trends observed in the shear-stress viscosity data and compare key results obtained from all the time points that were analyzed. Note that Figure 37 through Figure 40 represent samples taken on Day 30 of the test.

Figure 37 and Figure 38: In these plots, blue data lines (boxes) indicate viscosities read on the right-hand scale, and red data lines (circles) indicate shear stresses read from the left-hand scale. The behavior shown in these figures is typical of shear-thinning flow, where a yield stress needs to be overcome for flow to occur. Essentially, this means that at very low shear rates, the material exhibits high viscosities. Once enough stress is applied to the system to overcome the yield stress, the material begins to flow as a Newtonian fluid. According to the viscosimeter operator, this behavior could be evidence that a gel is forming or that, upon cooling, a sufficient amount of precipitation is available to cause an increase in viscosity. A water sample collected late in the test was examined after the precipitate settled in the water. This sample was taken of just the water above the settled precipitate (the so-called supernate), and that indicated that the supernate exhibited Newtonian behavior.

Figure 39: This plot compares the 25ºC viscosities of the 1220 series samples labeled 1220-F and 1220-U, which correspond to the filtered and unfiltered samples, respectively. Note that the filtered sample has lower shear stresses and viscosities than the unfiltered sample. When these results are compared with Figure 40, this behavior appears consistent with an increase in temperature, as well.

Figure 40: These results are representative of Newtonian flow, with secondary flow. The instrument parameters in the 1220 series of measurements were set at the lowest end of shear stress measurable by the Bohlin CS10 viscosimeter.

Figure 41 and Figure 42: These concurrent plots show viscosities for the 1800, 1206, 1214, and 1220 series at two different temperatures. The flow changes with the 1206, 1214, and 1220 series, and the viscosities increase as a function of time into the test. In addition, from the 1206 sample measured at 25ºC, the fluid exhibits non-Newtonian behavior that could be evidence that the system is gelling or that a significant amount of precipitation is occurring, thus causing an increase in the solids loading.

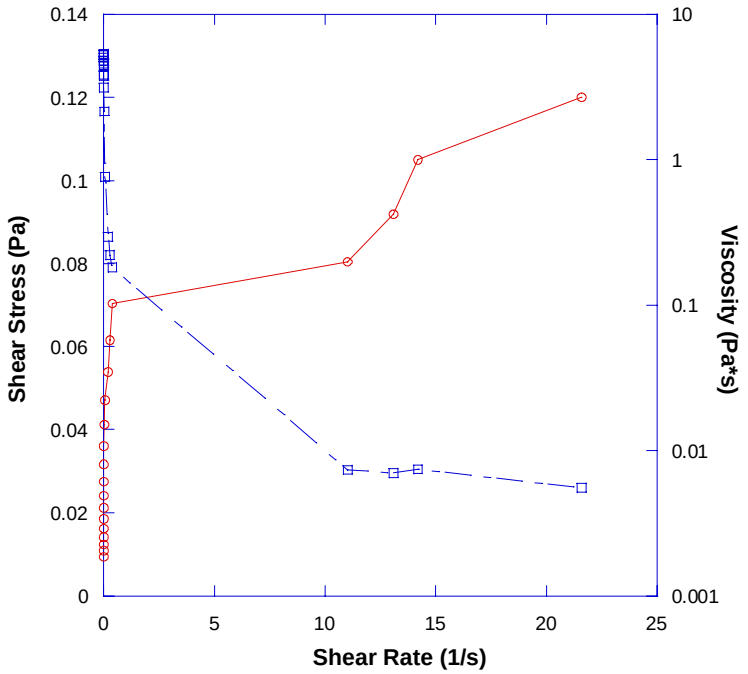

Figure 37. Sample 1220-U at 25ºC rheology. Blue data lines (boxes) indicate viscosity. Red data lines (circles) indicate shear stress.

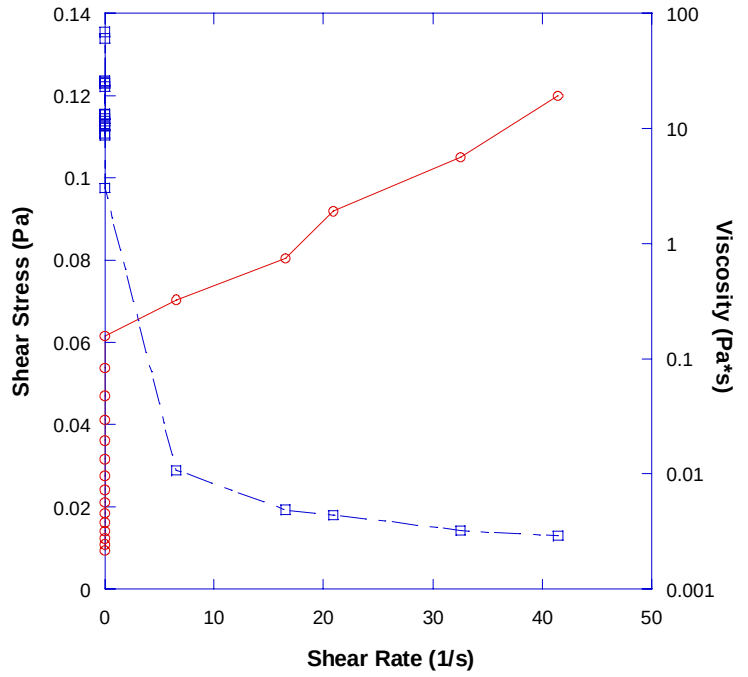

Figure 38. 1220-F at 25ºC rheology. Blue data lines (boxes) indicate viscosity. Red data lines (circles) indicate shear stress.

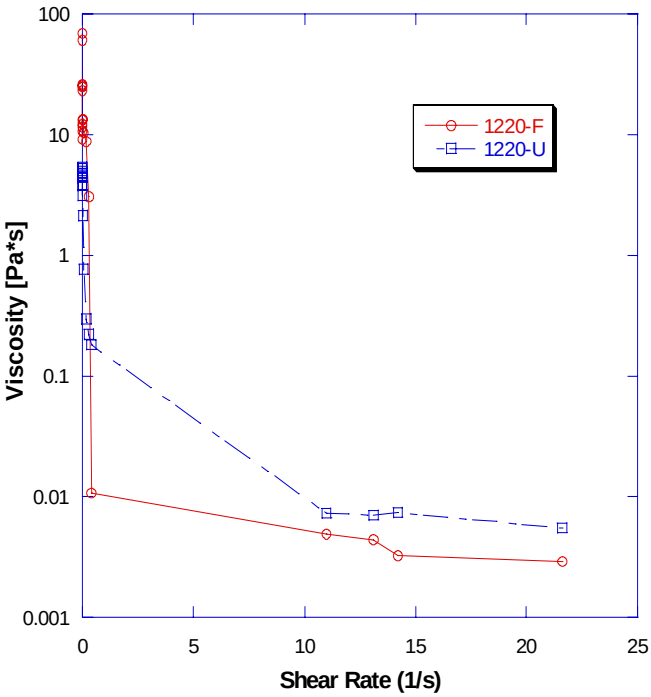

Figure 39. 1220 U and 1220 F viscosity series comparison at 25ºC.

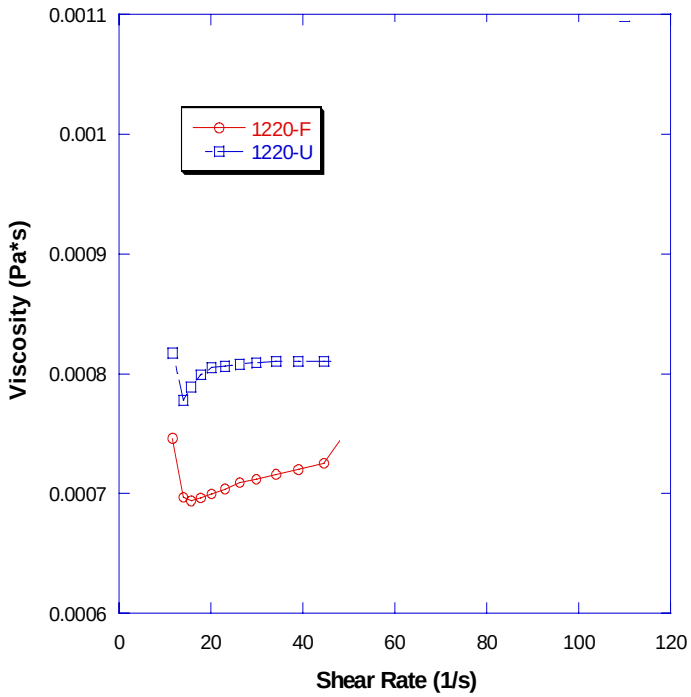

Figure 40. 1220 U and F series viscosity comparison at 60ºC.

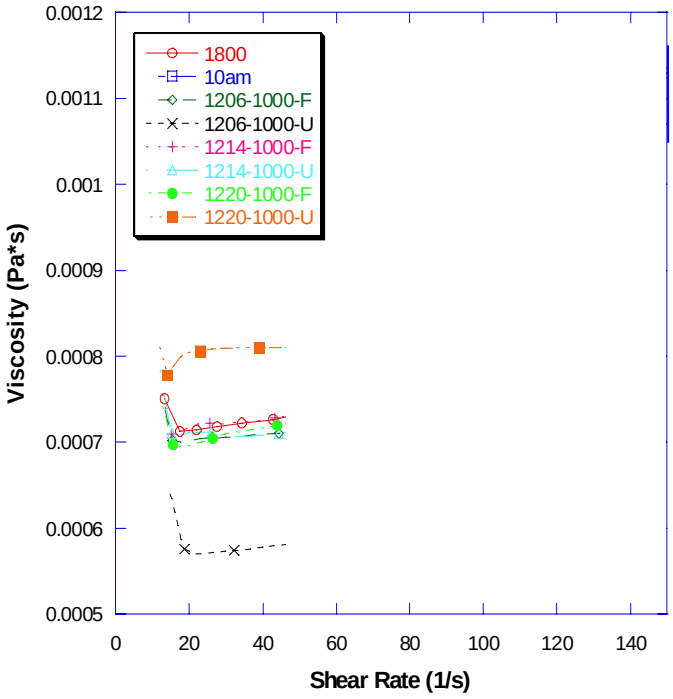

Figure 41. 60ºC viscosity aging study plot.

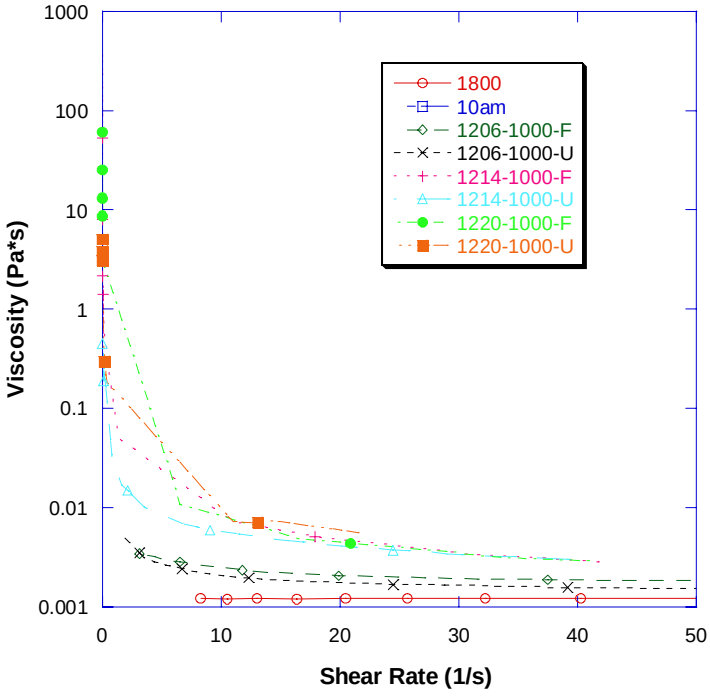

Figure 42. 25ºC viscosity aging study plot.

4.5.7 Metal Ion Concentrations

Metal ion concentrations in the daily water samples were analyzed by Assaigai Analytical Laboratories, Inc. (AALI), using inductively coupled plasma (ICP) spectroscopy. During the first 25 days of the test, both filtered and unfiltered samples were taken for analysis. Because of nondistinct differences between the filtered and unfiltered samples, only unfiltered samples were taken to be analyzed after Day 25 for the duration of the test. Filters used were Whatman GF/F glass microfiber filters with a 47-mm diameter and a nominal pore size of 0.7 micron. Individual metal concentration results are presented in Figure 43 through Figure 48.

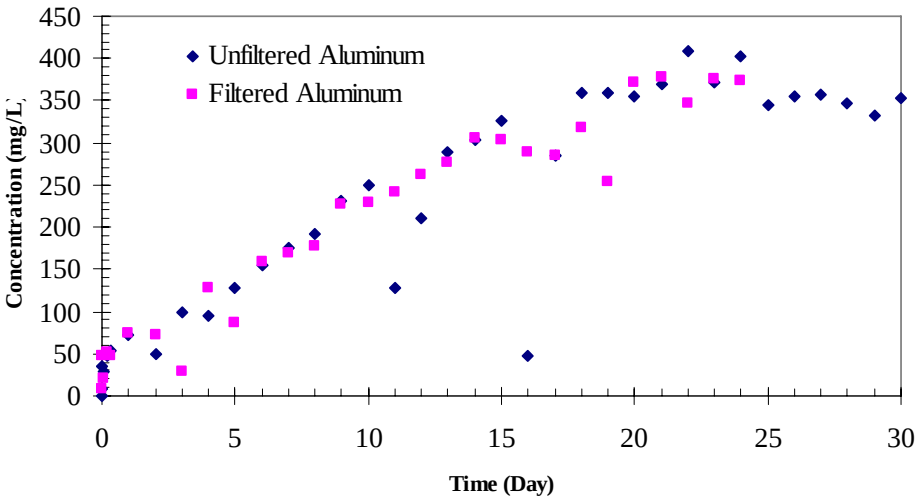

Figure 43. Aluminum concentration trend in ICET Test #1 daily water samples.

As seen in Figure 43, the aluminum concentration increased in a linear fashion over the test period until Day 16. After Day 18, the concentration appeared to level off at approximately 350 mg/L.

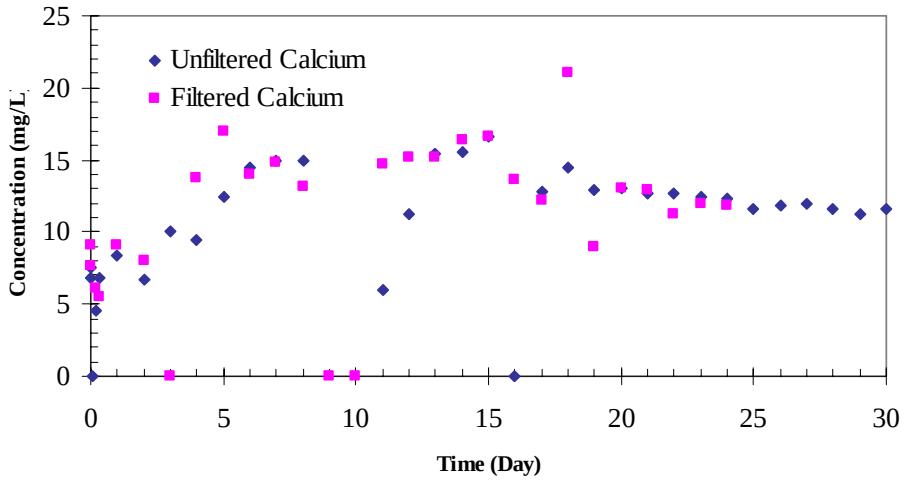

Figure 44. Calcium concentration trend in ICET Test #1 daily water samples.

Referring to Figure 44, the calcium concentration increased until Day 7, after which the concentration held somewhat constant until Day 13. From Day 13 to the end of the test, the calcium concentration decreased slightly to a value of 11.6 mg/L. As shown in Figure 45, the copper concentration remained moderately constant throughout the test.

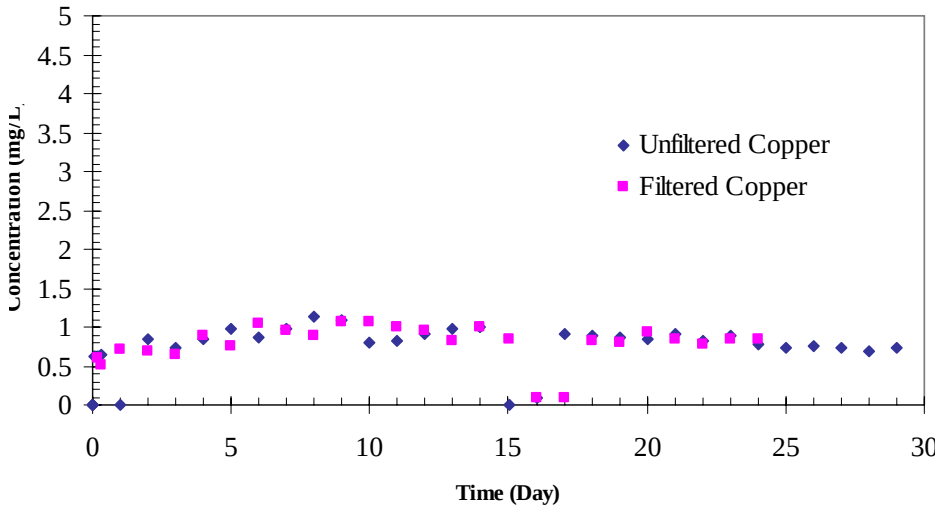

Figure 45. Copper concentration trend in ICET Test #1 daily water samples.

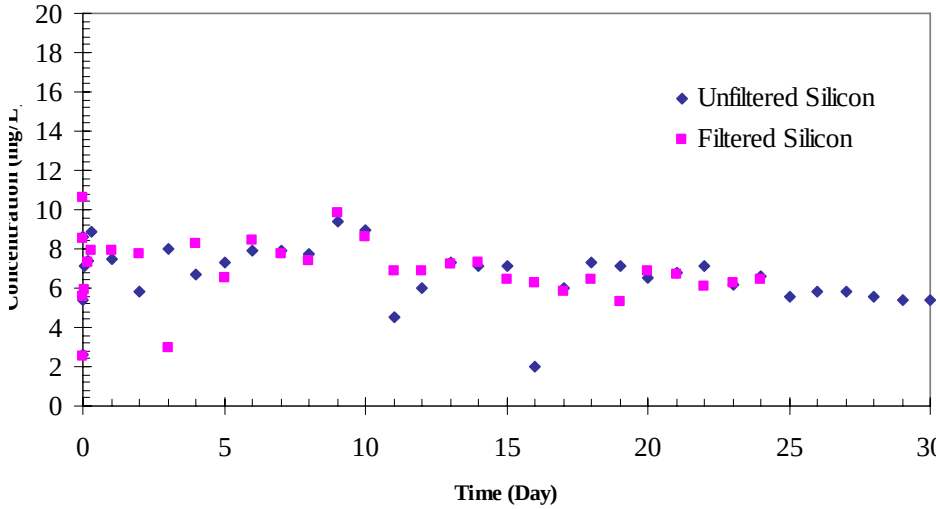

Figure 46. Silicon concentration trend in ICET Test #1 daily water samples.

Figure 46 shows that the silicon concentration was increased to approximately 10 mg/L at the beginning of the test. This concentration can be attributed to the addition of latent debris and fiberglass. The concentration stabilized at approximately 8 mg/L and gradually decreased over the duration of the test. It is apparent that silica concentrations in solution, as indicated by the presence of silicon, did not increase over time.

Figure 47 illustrates that the zinc concentration increased from 0.5 to 2 mg/L during the first day of the test. By the end of the first day, the concentration had decreased in an exponential fashion until it became undetectable on Day 13. It remained undetectable for the duration of the test. Sodium concentrations in solution remained relatively constant throughout the test, as shown in Figure 48.

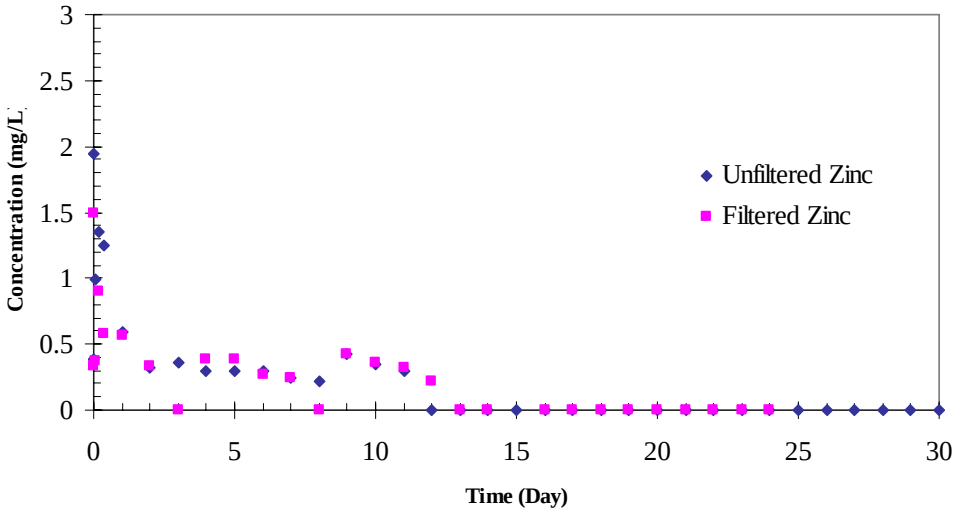

Figure 47. Zinc concentration trend in ICET Test #1 daily water samples.

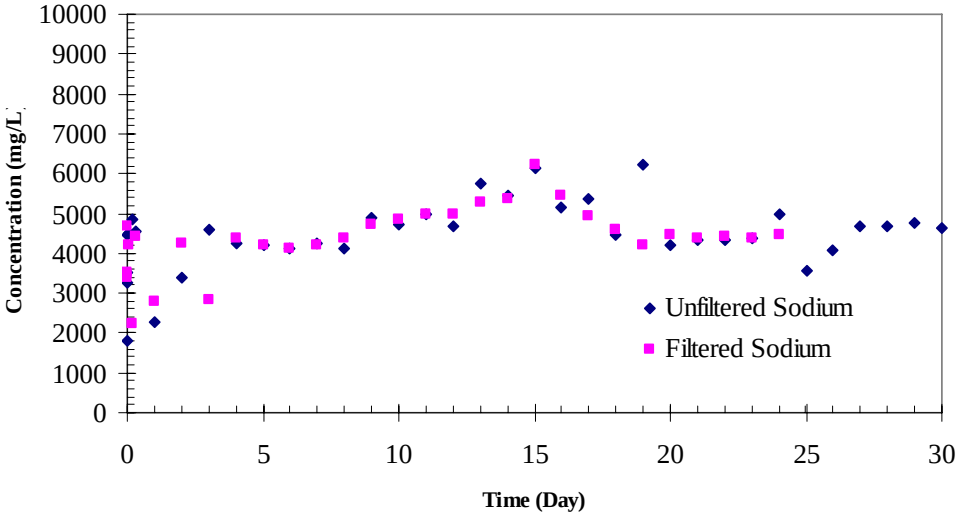

Figure 48. Sodium concentration trend in ICET Test #1 daily water samples.

Concentrations of various elements in the Metals I group, including chloride, boron, lithium, and potassium, were also monitored during the test. The first measurement was taken before the addition of NaOH spray, and the second measurement was taken after the NaOH spray. A third measurement was taken on Day 15, the middle of the test, and a fourth measurement was taken at the end of the test. As seen in Table 6, the experimental measurements were relatively constant throughout the test and within measurement uncertainties.

Table 6. Metal Concentrations for ICET Test #1

Time (Day)	Sample ID	Chloride	Boron	Lithium	Potassium
		mg/L			
0 (Before Spray)	ICET-1120-1703-U	80.3	3050	0.161	ND[a]
0 (Before Spray)	ICET-1120-1710-F	79.8	3120	0.19	ND
0 (After Spray)	ICET-1121-1035-U	81.4	2860	0.176	3.2
0 (After Spray)	ICET-1121-1035-F	82	2840	0.218	2.8
15	ICET-1206-1000-U	80.6	3090	0.34	9.1
15	ICET-1206-1000-F	82.1	2840	0.32	9.1
30	ICET-1221-800-U	78.6	2400	0.23	5.3
Min		78.6	2400	0.161	2.8
Max		82.1	3120	0.34	9.1
Standard Deviation		1.26	246.43	0.07	3.07

[a]ND = nondetect

4.6 Precipitated Solids

The most physically homogeneous samples extracted from the ICET experiment are those of the white chemical products formed in T1 solution upon cooling. This material is generically referred to as a "precipitate," but the exact physical formation mechanism has not been confirmed. Although consistent in appearance with a chemical flocculent formed via precipitation, the white material may also be formed by aggregation of smaller particles that are not visible at the test temperature or by nucleation upon small particles of other compounds that reside in solution at the test temperature.

Samples of filtered and unfiltered solution were collected in 250-mL plastic containers during each sampling episode and have been stored in the laboratory at ambient temperature. These samples were examined after being stored for several days. The initial samples (before initiation of the test) do not contain precipitate. The sample collected at 30 minutes into the test (after the NaOH addition was terminated) contains trace amounts of white precipitate, which can be seen if the bottle is gently tilted from side to side. However, the amount is so small that the precipitate is not visible on the bottom of the container. The 8-hour sample contains sufficient precipitate that the entire bottom of the bottle is coated with white precipitate. The quantity of precipitate appears to increase with each subsequent daily sample. The precipitate is a white, nearly neutrally buoyant material that qualitatively looks like aluminum hydroxide with boron. This precipitate does not appear to aggregate or coagulate into a cohesive mass, even after days of undisturbed settling. Only slight agitation is needed to remix the entire quantity into a uniform suspension with the supernate. A representative composition of this material is discussed in Section 4.6.2.

Sediment was observed on the bottom of the tank after the water column became less turbid. The material on the bottom of the tank is mostly white but with more color variation than the precipitate in the bottles. It also has a more granular appearance and is likely an agglomeration of the latent debris and concrete dust added to the tank, combined with a small quantity of the white precipitate observed in the bottles. No visible suspended precipitate was ever observed in the fluid inside the tank at the test temperature. Appendix H contains a more detailed evaluation of the tank sediment, including SEM images illustrating that a significant amount of fragmented fiberglass is also present in the settled debris.

4.6.1 TEM

The high resolution of the TEM, at least an order of magnitude greater than SEM, allows for qualitative size assessment of the underlying visible structures and aggregates. Small sample bottles of test solution were provided to the TEM laboratory, from which single drops of solution were extracted for examination. Settled precipitate was visible in most of the bottles that were transferred for TEM, and although the vials were not intentionally mixed before extracting droplets from the supernate, the semisolid particles visible in the following images represent suspended precipitate. The primary objective of TEM analysis is to determine whether the solids have a physical structure that is more consistent with microcrystalline flocculent or with amorphous hydrated gels. The TEM sample holder consists of a lacy carbon-coated grid that serves to suspend a liquid sample so that the diagnostic beam can be transmitted through the sample without interference from the sample mount. The sample grid is evident in many of the following images as a network of large sharply defined structures of uniform shading. In contrast, the appearance of suspended solids is very irregular, with much more color variation and evidence of structure on a much smaller scale than the sample grid.

Figure 49 presents a TEM image of a Day-15 filtered water sample that was allowed to cool to ambient temperature before examination. In fact, the TEM laboratory has no provisions for maintaining an in-situ sample temperature during analysis. From this figure, it appears that the larger aggregate structure comprises units of approximately 10 nm in diameter. After only 15 days of agglomeration and “aging,” smaller unit structures are still readily apparent.

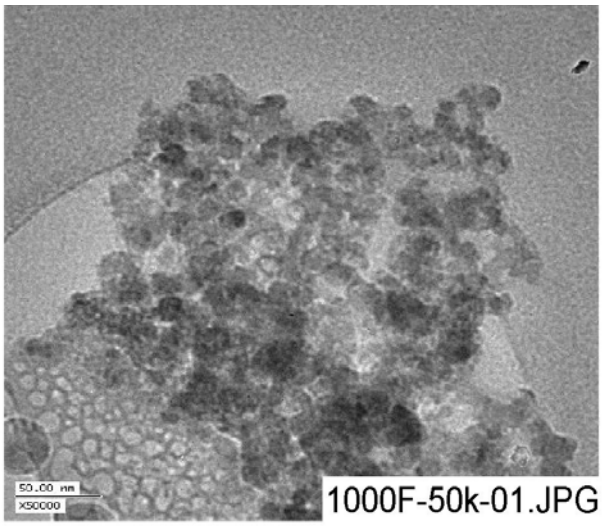

Figure 49. Electron micrograph magnified 50,000 times for the Day-15 filtered test sample.

Figure 50 through Figure 52 present comparisons of electron micrographs magnified by 4000, 10,000, and 50,000 times for the Day-30 unfiltered test samples. Increasing resolution reinforces the visual impression that suspended particulates with characteristic dimensions ranging from a few to tens of micrometers are actually agglomerations of globular nanoscale structures that may represent the characteristic minimal unit size of the aggregate. Similar comparisons for the Day-15 and Day-30 filtered test samples are presented in the appendices. Visual comparisons show that the Day-30 micrographs appear more granular than the Day-15 photographs. A comparison of Figure 49 and Figure 52 indicates a greater degree of aggregation in the Day-30 sample in that the basic structures are more uniformly packed.

It is unlikely that the precipitate material examined here will behave in the same manner as more familiar particulates such as iron oxide and silica-based soil with respect to its inherent head-loss properties. Furthermore, it would be difficult to estimate these properties based on geometric approximations that are based on particle size alone, given the difficulty of defining from these images a discrete physical element that would dominate flow resistance.

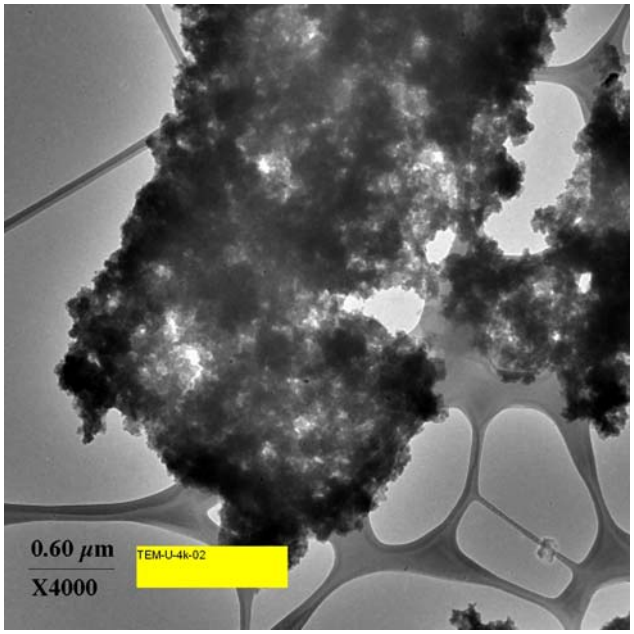

Figure 50. Electron micrograph magnified 4000 times for the Day-30 unfiltered test sample.

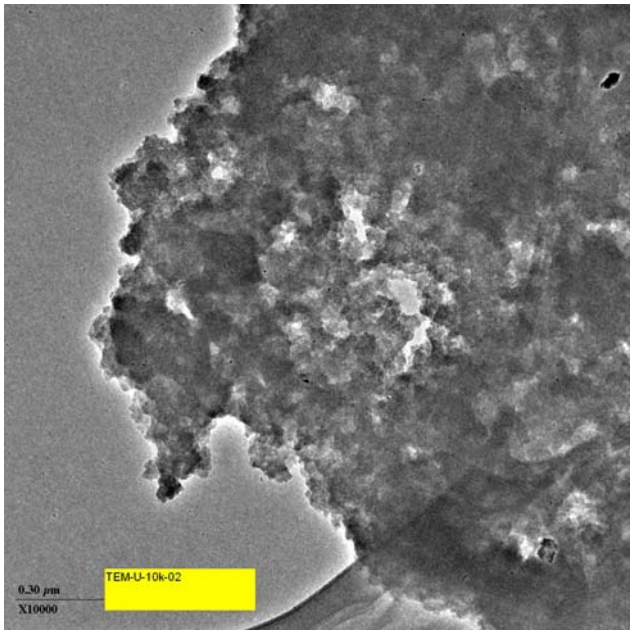

Figure 51. Electron micrograph magnified 10,000 times for the Day-30 unfiltered test sample.

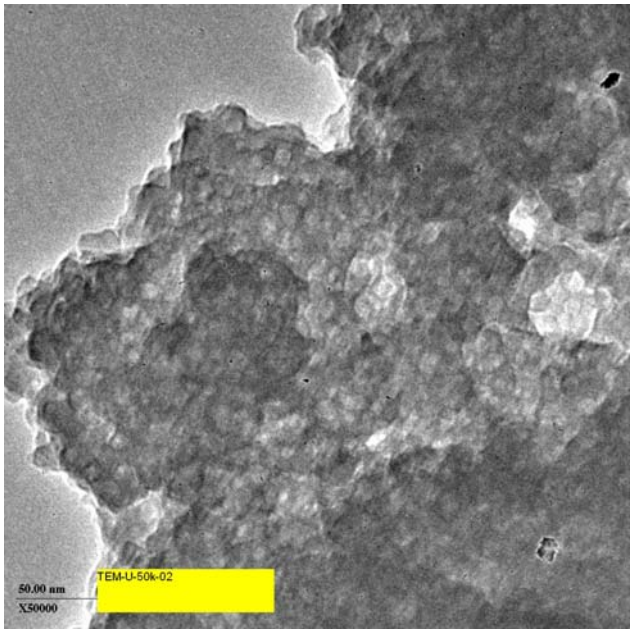

Figure 52. Electron micrograph magnified 50,000 times for the Day-30 unfiltered test sample.

Figure 53 and Figure 54 show TEM diffraction images magnified by 20 times for the Day-15 filtered and Day-30 unfiltered samples. The diffraction patterns represent structures present at one spatial location within an image such as those presented above. Some evidence of coherent diffraction patterns (bright spots) are observed at some sample locations, but no evidence of microcrystalline diffraction is observed at other locations (smooth uniform rings). In general, the TEM diffraction patterns are more similar to Figure 54. Filtered and unfiltered test samples show similar variations in transmission diffraction patterns,

suggesting that hot filtration either did not remove or did not prevent the formation of the suspend particulates identified in these examinations. TEM images for the Day-30 samples, which are included in the appendices of this report, show much less evidence of structure for the locations that were analyzed.

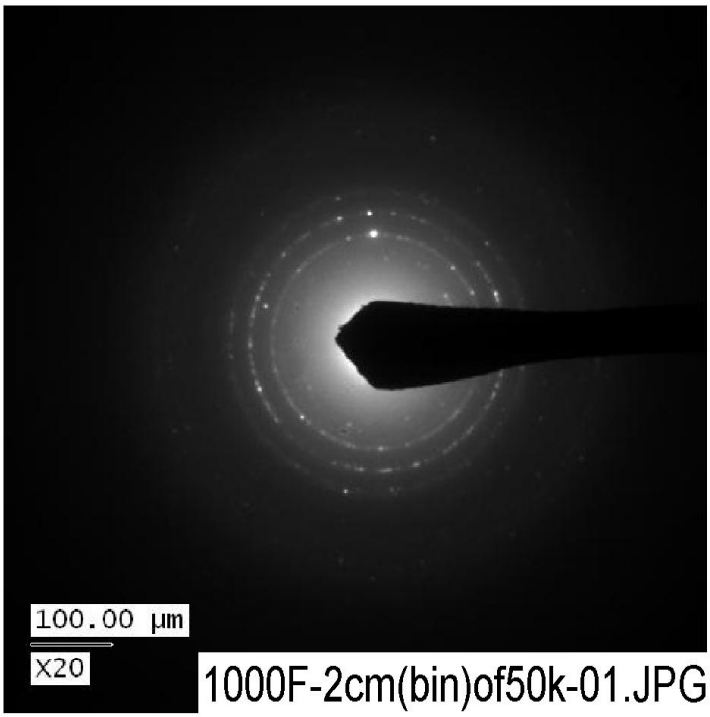

Figure 53. TEM image magnified 20 times for Day-15 filtered water sample.

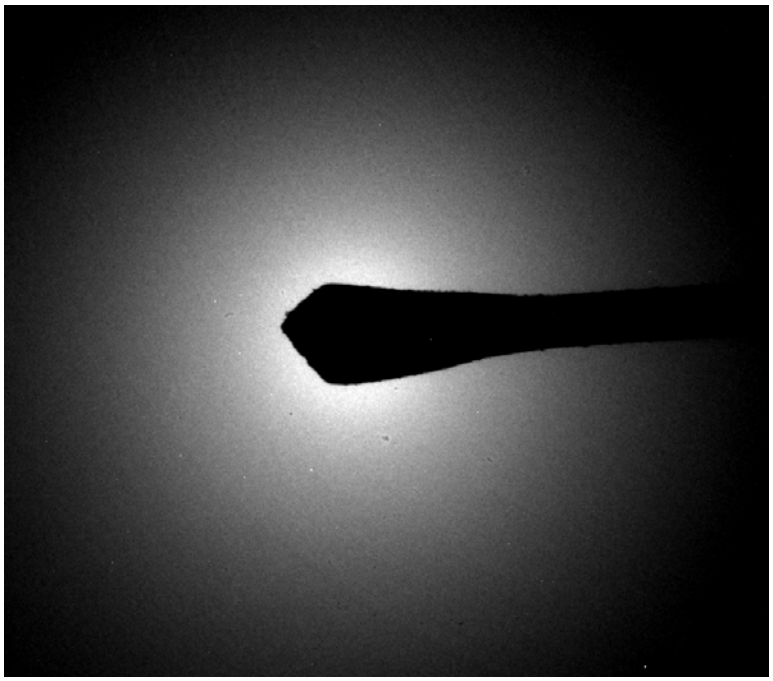

Figure 54. TEM micrograph magnified 20 times from the Day-30 unfiltered sample. (TEM-U-20cm-bin-03)

4.6.2 Additional Analytical Results

As described in Section 3.4, XRD, XRF, and ICP are potentially useful methods to determine compositions of materials. XRD is used to determine the composition and the structure of solid polycrystalline substances. This technique was used in an attempt to characterize two separate samples from Test #1. Figure 55 and Figure 56 present, for samples 1 and 2, respectively, data from XRD examinations of the post T1 sludge that was obtained upon draining and storage of the effluent. The sludge examined in Figure 55 was dried in stages within a small liquid sample bottle containing suspended material using a 50°C hotplate. One sample of semidry paste was extracted for examination, and then the remainder was dried more completely and powdered for the x-ray mount. The bottom pattern shown in Figure 55 corresponds to the moist paste, whereas the top pattern corresponds to the dried then powdered sludge.

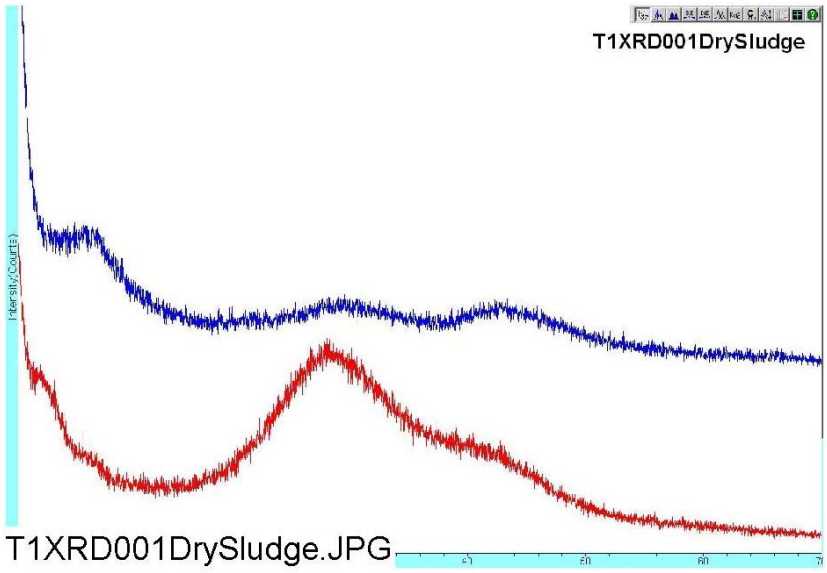

Figure 55. Intensity vs scattering angle for post-T1 dry sludge (sample 1), bottom–moist paste, top–dry powder.

A second sample of the precipitate was air dried overnight in a convection oven at approximately 38°C. Figure 56 presents the XRD analysis results for this sample, which exhibits a significant amorphous component along with tincalconite and borax at a ratio of ~90:10 weight percent of tincalconite to borax.

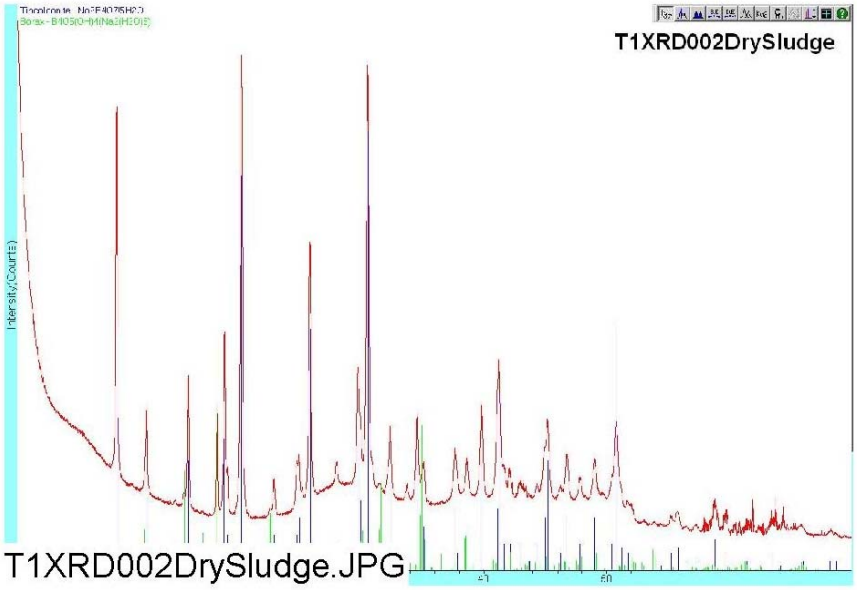

Figure 56. Intensity vs scattering angle for post-T1 dried sludge (sample 2).

As may be seen from a comparison of Figure 55 and Figure 56, one of the samples exhibited a crystalline structure with the characteristic scattering properties of tincalconite superimposed on an underlying amorphous trend, whereas the other sample was wholly amorphous in nature. Additional investigations are necessary to determine the exact origin of the difference, but thermal history clearly plays a role in determining the structural configuration at the time of examination.

XRF was also used to determine, both qualitatively and quantitatively, the elemental composition of the precipitates from Test #1. The elemental composition of solid samples is obtained from XRF instead of specific substances (i.e., compounds). The results of this testing indicate that the precipitates of Test #1 were mainly composed of Na, Al, Ca, and Si. The accuracy of the results depends on how closely the comparative standards resemble the sample. Also, the sensitivity of XRF decreases with decreasing atomic weight, so it is normally difficult to identify an element with an atomic number that is less than that of carbon.

Table 7 presents an elemental summary of the ICP analysis for the precipitate. This analysis is reflective of the typical test analysis performed during Test #1, with the exception of carbonates. All elements, except for carbonates, were analyzed by ICP-AES. The carbonate value was obtained by titration using EPA method 310.1.[23] The elements detected accounted for 55%, 84%, and 78% of the total sample composition. The precipitate is largely composed of carbonate, aluminum, boron, and sodium, which can be seen in Table 8. The remainder consists of elements not detected by ICP, which notably includes oxygen.

Table 7. Composition of Precipitates

Element	mg/kg		
	11/27 Precipitate (Day 6)	**12/08 Precipitate (Day 17)**	**12/17 Precipitate (Day 26)**
CO_3^{2-}	208,000	169,000	217,000
Al	38,600	99,600	89,200
B	125,000	202,000	139,000
Ca	3980	3800	3660
Cu	145	126	118
Fe	ND[a]	5	ND
Pb	ND	ND	ND
Li	9	9	ND
Mg	63	34	28
Ni	1	1	2
K	310	354	359
Si	733	754	422
Zn	76	6	ND
Na	170,000	363,000	334,000
Wt % of Total Sample	55	84	78

[a]ND = nondetect.

Table 8. Main Elemental Components of Precipitate

Element	Mass % of Detected Sample			
	11/27 Precipitate (Day 6)	12/08 Precipitate (Day 17)	12/17 Precipitate (Day 26)	Average Precipitate
CO_3^{2-}	38	20	28	29
Al	7	12	11	10
B	23	24	18	22
Na	31	43	43	39
Other	1	1	1	1

Table 9 presents an elemental summary of the ICP analysis for the filtered precipitate. The glass fiber filter was digested with the filtered precipitate; thus, the weight percent includes the filter. However, the ICP results of the filtered precipitate have been corrected to help eliminate any elemental contribution from the digested glass fiber filter. This correction was done by performing ICP-AES elemental analyses on a blank filter from the same batch of filters as that used for the filtered precipitate. The results of that analysis were subtracted from the overall results of the filtered precipitate. It appears that the filtered precipitate is largely composed of sodium, boron, and aluminum.

Table 9. Filtered Precipitate ICP Results

Element	mg/kg		
	11/27 Filtered Precipitate (Day 6)	12/08 Filtered Precipitate (Day 17)	12/17 Filtered Precipitate (Day 26)
Al	351	3,989	641
B	6864	5935	5863
Ca	ND[a]	ND	ND
Cu	ND	ND	ND
Fe	ND	ND	ND
Pb	ND	ND	ND
Li	ND	ND	ND
Mg	ND	ND	ND
Ni	ND	ND	ND
K	ND	ND	ND
Si	551	285	321
Zn	ND	ND	ND
Na	12,275	4511	13,055
Wt % of Total Sample	2	1	2

[a]ND = nondetect.

Table 10 presents the ICP results for the test sediment, concrete, dirt, and fiberglass insulation. The concrete, dirt, and fiberglass-insulation ICP results were performed in attempts to normalize the sediment results to produce a qualitative composition. Because very small amounts of the dirt and concrete were added to the tank, their contribution may be negligible, although their compositions were of interest. The sodium concentration of the sediment was not provided; thus, the results were not normalized because it was assumed, based on the composition of the previous precipitates, that sodium may be a major part of

the sediment composition. Further analysis of the sediment must be performed before any definite conclusions can be reached.

Table 10. Solid Sample and Reference ICP Results

Element	mg/kg			
	Fiberglass Insulation	**Dirt**	**Concrete**	**Sediment**
Al	114	7230	2770	6460
B	1440	NA[b]	8	3750
Ca	3920	9820	47,300	3090
Cu	ND[a]	34	112	744
Fe	201	12,200	3120	6100
Pb	4	9	4	32
Li	3	6	3	12
Mg	1100	2290	905	883
Ni	ND	7	5	327
K	526	926	434	153
Si	110	965	1850	670
Zn	11	42	30	5600
Na	10,100	868	474	NA
Wt % of Total Sample	1.75	3.44	5.70	3

[a]ND = nondetect.
[b]NA = not applicable.

The elemental composition of the precipitate has been investigated by EDS, XRF, and ICP spectroscopy. Substantial variability in measured elemental concentrations was observed between samples analyzed with the same method and between diagnostic methods applied to the same sample. A survey of these measurements was performed to recommend suitably averaged mass proportions for the dominant constituents that were observed (see Table 11).

Table 11. Elemental Composition (wt %) of 30-Day High-Volume Filtrate

Element	Method		
	EDS	**ICP**	**XRF**
O	48	–	45
Al	11	11	7
Ca	2	0.4	0.8
Na	16	43	24
B	21	18	–
CO_3^{2-}	–	28	–
$H_2O + CO_2$	–	–	34